J Nanopart Res (2020) 22: 308
https://doi.org/10.1007/s11051-020-05038-8

RESEARCH PAPER

Synthesis of early transition metal oxide nanomaterials and their conversion to nitrides

Anastasia M. Kastl · Andrew P. Purdy · Raymond J. Butcher

Received: 23 December 2019 / Accepted: 2 October 2020 / Published online: 13 October 2020

Abstract The synthesis of nanorods and nanowires of early transition metal oxides by hydrothermal methods and the conversion of some bulk oxides to nitrides in NH_3 flow are both well established. However, the conversion of such oxide nanostructures to nitrides is not as well explored but could be a valuable method of producing nanowires, nanorods, and other asymmetric or high aspect ratio nanoparticles of the highly conductive metal nitrides. In this work, nanostructures of TiO_2, V_2O_5, MoO_3, and WO_3 and mixtures thereof were synthesized by hydrothermal reactions, and conversion into nitride was attempted by heating the oxide material under NH_3 flow with or without N_2 flow. It was found that slow heating produces the best shape retention, but the nitridized products are porous in even the most favorable cases. The products were characterized by X-ray powder diffraction and scanning electron microscopy. Two-point conductivity measurements were done on the nitride materials, and optical measurements to characterize the plasmon absorption were done in favorable cases.

Keywords Nanowires · Nanorods · Titanium dioxide · Vanadium oxide · Molybdenum oxide · Tungsten oxide · Titanium nitride · Vanadium nitride · Molybdenum nitride · Nitridation · Hydrothermal reactions · Crystal structures

Introduction

Most of the nitrides of the early transition metals are refractory materials with metallic electrical conductivity and in the case of TiN is actually more conductive than elemental Ti (Lengauer et al. 1995). Conductive nanowires are useful for a number of purposes such as the preparation of conductive transparent composites (Zhang and Engholm 2018; Lang et al. 2020), and inexpensive methods of bulk preparation of conductive nitride nanowires are desirable. Few methods exist for the direct synthesis of metal nitride nanowires (for some, see Joshi et al. 2005; Ding et al. 2013), but most of the early transition metal oxides, with the exception of ZrO_2 and HfO_2, can be converted to the nitrides by heating at 1200 °C or less under flowing NH_3 (Gou et al. 2017; Mangamma et al. 2007; Howell et al. 2018; Tan et al. 1994; Sharma et al. 2001; Lerch 1996; Yu et al. 1998; Mosavati et al. 2016; Mosavati et al. 2017). The synthesis of early transition metal oxide nanowires by

Electronic supplementary material The online version of this article (https://doi.org/10.1007/s11051-020-05038-8) contains supplementary material, which is available to authorized users.

A. M. Kastl
NREIP Intern, Chemistry Division, Naval Research Laboratory, Washington 20375 DC, USA

A. P. Purdy (✉)
Chemistry Division Code 6100, Naval Research Laboratory, Washington, DC 20375, USA
e-mail: andrew.purdy@nrl.navy.mil

R. J. Butcher
College of Arts & Sciences, Professor of Inorganic & Structural Chemistry, Howard University, Washington, DC 20059, USA

hydrothermal methods (Chen and Mao (2007), Wang et al. (2014)) in acidic (Perales-Martínez and Rodríguez-González 2017; Zhou et al. 2011; Cassaignon et al. (2007)) or alkaline solution has been described extensively (Hirao and Hasegawa 2010; Poudel et al. 2005; Zhang et al. 2010; Wei et al. 2006). What has not been explored as much is the conversion of these oxide nanowires to nitride nanowires. Most of the research done in this area consists of small quantities grown on a substrate and then annealed under NH_3 flow to convert the oxide to a nitride (Qiu et al. 2010; Xihong et al. 2013) or production of bulk powders where particle shape was not a consideration (Drygas et al. 2006; Fei et al. 2011; Zhou et al. 2017). This has been successfully done but sometimes with poor shape retention. Since there is a net loss of atoms when converting oxides to nitrides, crumbling, porosity, or shrinkage would be expected to occur. Less research has been done on the conversion of bulk early transition metal oxide nanostructures to nitrides through a similar annealing method, which would allow for the bulk production of metal nitride nanorods or nanowires (Xiao et al. 2013; Song et al. 2014). Intriguingly, some reports describe excellent shape retention upon nitride conversion, as bulk TiO_2 crystals were converted to porous TiN single crystals (Lin et al. 2018) and TiO_2 nanostructures were converted to tubular TiN nanostructures (Zhang et al. 2017). In this work, we had the objective of preparing bulk quantities of metallic early transition metal nitride nanowires. To do this, we prepared nanorods and nanowires of titanium, vanadium, molybdenum, and tungsten oxides (and mixtures thereof) by hydrothermal methods and explored the conditions for nitride conversion with maximum shape retention.

Experimental

Oxide synthesis

All reagents were used without further purification: titanium dioxide 21 nm powder (Aldrich #718467 99.5%), sodium tungstate dehydrate (Fisher), ammonium vanadate (Fisher), titanium tetrachloride (Aldrich), sodium vanadate (Johnson Matthey 98%), and sodium molybdate (Aldrich 99 + %). All air-sensitive or extremely volatile reagents or products were handled in a dry box under argon or in a flow box under nitrogen, respectively. All water used in any reaction was distilled water. All metal oxide syntheses were carried out in a ~ 20 mL Teflon cup inside an acid digestion bomb (Parr 23 mL High Pressure Acid Digestion Bomb Model 4746) except for three alkaline reactions as denoted in Table 1. Reactions **10** -**11** were carried out in a 1″ dia PTFE test tube inside a Newport Scientific preliminary test vessel assembly (cat # 41-19320) under autogenous pressure and **9** in a Teflon beaker in a Si oil bath with a watch glass on top to limit evaporation. The metal oxide source compound was added to water and stirred. The remaining reagents were then added in the appropriate fashion as indicated in Table 1. The vessel was then heated to a temperature between 110 and 215 °C for 20 h to 13 days. The resulting product was then washed with water, ethanol, and, in particular reactions, nitric acid to obtain the necessary neutralization.

Phosphonic acid synthesis was done in a manner similar to Vallant et al. 1998. (a) $P(OEt)_3$ (55 g, 331 mmol) and $C_{14}H_{29}Br$ (37.5 g, 135 mmol) was heated under N_2 flow for 36 h at 110 °C and 3 h at 180 °C. Then, 100 mL concentrated HCl was added and mixture refluxed for 1 day and allowed to cool. The solids were filtered and washed with water and MeCN. Recrystallization from MeCN did not work, so product was recrystallized from $CHCl_3$ and pumped dry. A total of 21.87 g $C_{14}H_{29}PO_3H_2$ (58%) was isolated. NMR: (^{31}P, MeOH solution) 30.88 ppm. (b) Under N_2 flow, 60 g (361 mmol) $P(OEt)_3$ was heated to 180 °C, and $C_9H_{19}I$ (36.84 g, 145 mmol) was added in 3–5 mL portions, with the volatiles (presumably EtI) allowed to clear before adding the next increment. After addition, allowed to stir for 12 h at 160 °C. Then refluxed with 100 mL conc HCl for 1 d, let cool, and extracted top layer with pentane, rotovapped, and material was recrystallized from hot MeCN. Product was filtered, washed with cold MeCN, and dried under vacuum. A total of 8.77 g (29%) $C_9H_{19}PO_3H_2$ was isolated. NMR: (^{31}P, MeOH solution) 30.95 ppm.

Nitride synthesis

All nitridation reactions were completed in an alumina boat in a 1 in. OD quartz tube. The tube was heated by a silicon carbide heating element in a horizontal tube furnace with a 6 in. hot zone. The nitrogen and anhydrous ammonia used in these reactions were supplied by Air Products. The nitrogen was supplied by the boil-off from in-house stored liquid nitrogen, and the anhydrous ammonia was stored in and obtained from a container

Table 1 Reaction reagents and conditions for all hydrothermal metal oxide syntheses

#	Metal source	Water (g)	Other	Time (*D*)	Temp (°C)	Products[g]	Yield
1	1.00 g NH_4VO_3	7.0	0.50 g HNO_3	4	215	V_2O_5, $H(V_3O_8)$ H_2O	
2	$V(OH)_2NH_2$[a]	~ 10	1.17 mL 0.1 M HNO_3[b]	1.3	215	VO_2, V_2O_5, $H_4V_2O_4$	
3	0.2 g NH_4VO_3	45	5 mL EtOH, drops HCl[b]	1.04	185	VO_2, V_2O_5	81%
4	0.6 mL $TiCl_4$[b]	7.0	–	4	215	Rutile (TiO_2)	
5	0.6 mL $TiCl_4$[b]	6.0	1.0 mL NH_4OH[b]	2	215	Rutile (TiO_2)	
6	1.12 g $TiCl_4$[b]	6.0	–	13	215	Rutile (TiO_2)	
7	1.16 g $TiCl_4$[b]	6	0.10 g C_{14}Phosphonic acid	6	215	Rutile (TiO_2)	
8	1.16 g $TiCl_4$[b]	7	0.07 g C_9 Phosphonic acid	6	215	Anatase & Rutile (TiO_2)	
9[c]	2.6 g TiO_2	–	73.74 g 8.2 m NaOH	0.83	110	Anatase & Rutile $H_2Ti_2O_5$ H_2O	98%
10[c]	1.0 g TiO_2	–	35.02 g 8.2 M NaOH	3	165	$Na_2Ti_3O_7$	97%
11[c]	1.02 g TiO_2	–	35.08 g 8.2 M NaOH	1.17	155	$H_2Ti_2O_5$ H_2O	100%
12A/ 12B	1.32 g $TiCl_4$[b], 0.81 g NH_4VO_3	7.10	–	5	215	(A) V_2O_5, $H_{0.39}V_2O_5$; (B) Anatase (TiO_2)	
13	1.06 g $TiCl_4$[b], 0.22 g NH_4VO_3	5	–	3	215	TiO_2	92%
14A/ 14B	1.12 g $TiCl_4$[b], 1.04 g NH_4VO_3	5	–	4.5	215	(A) V_2O_5, $H_{0.39}V_2O_5$; (B) Anatase	32%
15	1.00 g $TiCl_4$[b], 0.64 g NH_4VO_3	5	–	3	215	Anatase (TiO_2)	36%
16	2.66 g Na_2MoO_4	5.16	2.69 g HNO_3	4	215	$H_{0.34}MoO_3$(?), MoO_3	
17	0.04 g Na_2WO_4 H_2O	9	1 mL EtOH, drops HCl[d]	1.04	185	WO_3, $WO_3(H_2O)$	83%
18	1.0 g NH_4VO_3, 2.81 g Na_2WO_4 H_2O	5	8.6 g HCl[e]	3	215	$W_{1.5}O_{4.5}2(H_2O)$[f]	37%

[a] Precursor made from 45 mL H_2O stirred with 0.23 g NH_4VO_3, 1 mL HCl dropwise, 3 mL N_2H_4 H_2O, stirred for ½ hr, and centrifuged then sonicated in 30 mL DI H_2O (Wu et al. 2011)

[b] Reagent was added dropwise into solution

[c] Alkaline reaction washed with water then 0.1 M HNO_3 then with water until pH was 7 (Hirao and Hasegawa 2010)

[d/e] HCl added dropwise until pH was 2 or between 6 and 8, respectively

[f] The wash solution produced yellow chunky ($Na_3(NH_4)_2V_3W_3O_{19}$ $12H_2O$) crystals and clear needle-like crystals ($NaVO_3$ $2H_2O$), and the structures were determined by single crystal X-ray crystallography

[g] JCPDS Cards: Anatase 1-84-1285, 4-477; Rutile 1-83-2242; $H_2Ti_2O_5$ H_2O 47-124; $Na_2Ti_3O_7$ 59-666; VO_2 1-79-1655; V_2O_5 1-76-1803; $HV_3O_8(H_2O)$ 1-76-6608; WO_3 1-85-2459; $WO_3(H_2O)_{0.33}$ 1-87-1203; $W_{1.5}O_{4.5}(H_2O)_2$ 1-81-779; MoO_3 1-78-4613, 1-706; $H_{0.39}V_2O_5$ 38-0009; $H_4V_2O_4$ 1-88-2026; $H_{0.34}MoO_3$ 34-1230

with a sodium amide drying agent in all reactions except **21**. Both of these gasses passed through a ¼ in. piping manifold into the tube, and exited through a silicon oil bubbler which was vented to a fume hood.

In a typical reaction, a small amount of metal oxide was placed in the alumina boat which was placed on top of a glassware oven to air-dry. The boat was then placed in the quartz tube in the center of the tube furnace. If the sample was dried, only nitrogen gas flowed through the furnace initially, and ammonia was added later. The temperature was manually raised, via a controller, by differing rates, up to 800 or 900 °C and allowed to nitride at that temperature for differing amounts of time as seen in Table 2.

Analysis and characterization

All product compositions were analyzed using XRD powder patterns from a Rigaku SmartLab 2080B212 3 kW powder X-ray diffractometer with Cu Kα radiation. The air-sensitive products were analyzed using an inert atmosphere sample holder with a Kapton window. All product nanostructures and some compositions were analyzed using a LEO-1550 FE-SEM to obtain SEM images and EDS data. Nitrides that appeared to be nanowires or nanorods were further analyzed through UV-Vis and IR spectra for samples that would suspend in ethanol or methylene chloride, respectively. Nitrogen BET analysis was done on some oxide and nitride product pairs on a Micromeritics ASAP 2020 absorption analyzer. Preliminary electrical conductivity measurements of the nitride products were done by placing a weighed small amount in a quartz tube sandwiched between two 5/32″ diameter steel rods, with the quartz tube clamped vertically, and a weight of 1192 g was placed on the top rod to put a consistent pressure on the sample, and the height was measured. A Fluke 111 multimeter was used to measure low voltage DC resistance, an Amprobe AMB-40 megohmmeter was used to measure high voltage resistance, and a BK Precision 878 LCR meter was used to measure capacitance and resistance at 1 KHz and 120 Hz. Because of the capacitance in **22** and **23**, the oxide nanowires **11** were measured as well. The data are presented in Table 5. Raman spectra were measured on a Renishaw InVia Raman Microscope with a 514 or 785-nm excitation laser.

Results and discussion

Oxide nanorod and nanowire synthesis

Acidic hydrothermal reactions that made short TiO_2 nanorods were done by adding $TiCl_4$ to water, adding optional additives including NH_4OH or long-chain phosphonic acid surfactants, and cooking the mixture hydrothermally in a Teflon acid digestion bomb at 215 °C (Table 1, **4**–**8**). In all cases, agglomerated spherical structures composed of short TiO_2 nanorods or

Table 2 Nitriding conditions for the conversion of several metal oxides to metal nitrides

#	Oxide source	Gas	Drying rate	Temp NH_3 added	Nitriding rate	Temp (°C)	Time (h)	Products	Yield
19	TiO_2 (**4**)	NH_3	None	–	None	800	16	TiN	
20	TiO_2 (**7**)	NH_3, N_2	None	–	None	800	2	TiN, rutile	83%
21	TiO_2 (**7**)	NH_3, N_2	100 °C/30 min	200 °C	100 °C/30 min	800	3	TiN	88%
22	TiO_2 (**10**)	NH_3[c],N_2	100 °C/h	300 °C	100 °C/h	800	2	TiN	98%
23	TiO_2 (**11**)	NH_3[d],N_2	100 °C/h	300 °C	100 °C/h	800	7	TiN	76%
24	V_2O_5, $H(V_3O_8)$ H_2O (**1**)	NH_3, N_2	b	800 °C	b	900	1.5	V_2O_3, VN	
25	V_2O_5, $H_{0.39}V_2O_5$ (**14A**)	NH_3, N_2	c	100 °C	100 °C/h	900	16.5	VN	66%
26	VO_2 (**3**)	NH_3, N_2	100 °C/30 min	300 °C	100 °C/h	900	15	VN	90%
27[4]	MoO_3 (**16**)	NH_3,N_2	100 °C/h	200 °C	100 °C/30 min	800	1	Mo_2N	89%

[a] No sodium amide drying agent used

[b] Dried at 800 °C, NH_3 added (½ h at 800 °C) then up to 900 °C (1 h)

[c] Dried at 100 °C (½ h), 250 °C (½ h), and then 400 °C (1 h; start of const. ramping)

[d] Left overnight at 300 °C before nitriding

nanoparticles were formed, which were usually rutile phase, except for **8**. Both **7** and **8**, to which phosphonic acid surfactants were added, had more elongated nanorods than **4**–**6**. SEM images of representative examples are shown in Fig. 1. Similar type structures have been reported by others from hydrothermal reactions involving Ti compounds in acidic media and are often described as nanoflowers (Perales-Martínez and Rodríguez-González 2017; Zhou et al. 2011; Cassaignon et al. 2007). Raman spectra (supporting information) are consistent with the XRD analysis except that the materials produced with phosphonic acids, **7** and **8**, showed very high fluorescence at 514-nm excitation and had to be observed with a 785-nm laser to see the weak spectra. The most likely reason for this fluorescence is incorporation of phosphonate into those materials.

Since longer TiO_2 nanowires were desired, alkaline synthesis reactions were used as well (Hirao and Hasegawa 2010). For these reactions **9**–**11**, a commercially available TiO_2 nanomaterial was subjected to hydrothermal conditions with an ~ 8 M NaOH solution, followed by washing with dilute HNO_3 and water. As expected, long nanowires grew. Reactions **9** and **10** both formed distinct nanowires with diameters from 10 to 150 nm and lengths from 300 to 12 μm. The wires in **9** are much thinner and longer than those in **10**, but **9** did not go to completion and a lot of the starting TiO_2 material remained (Fig. 2). This difference is most likely due to the higher temperature and longer reaction time in **10**. Reaction **11** was done at a slightly lower temperature and less time than **10**. SEM images are shown in Fig. 2, and XRD powder patterns for the TiO_2 nanomaterials are shown in Fig. 3. The powder pattern of **10** has the closest resemblance to $Na_2Ti_3O_7$ (JCPDS 00-59-666), possibly as a result of incomplete acid washing, and **9** and **11** had very broad XRD lines that had the closest match to a hydrous titanium oxide (JCPDS 00-47-124). Heating **11** at 140 °C sharpened the broad XRD peaks a bit, and even heating under vacuum at 250 °C or 400 °C caused a mass loss of 28% (presumably water loss), but no change in the powder pattern, and very little change in the Raman spectra (supporting information).

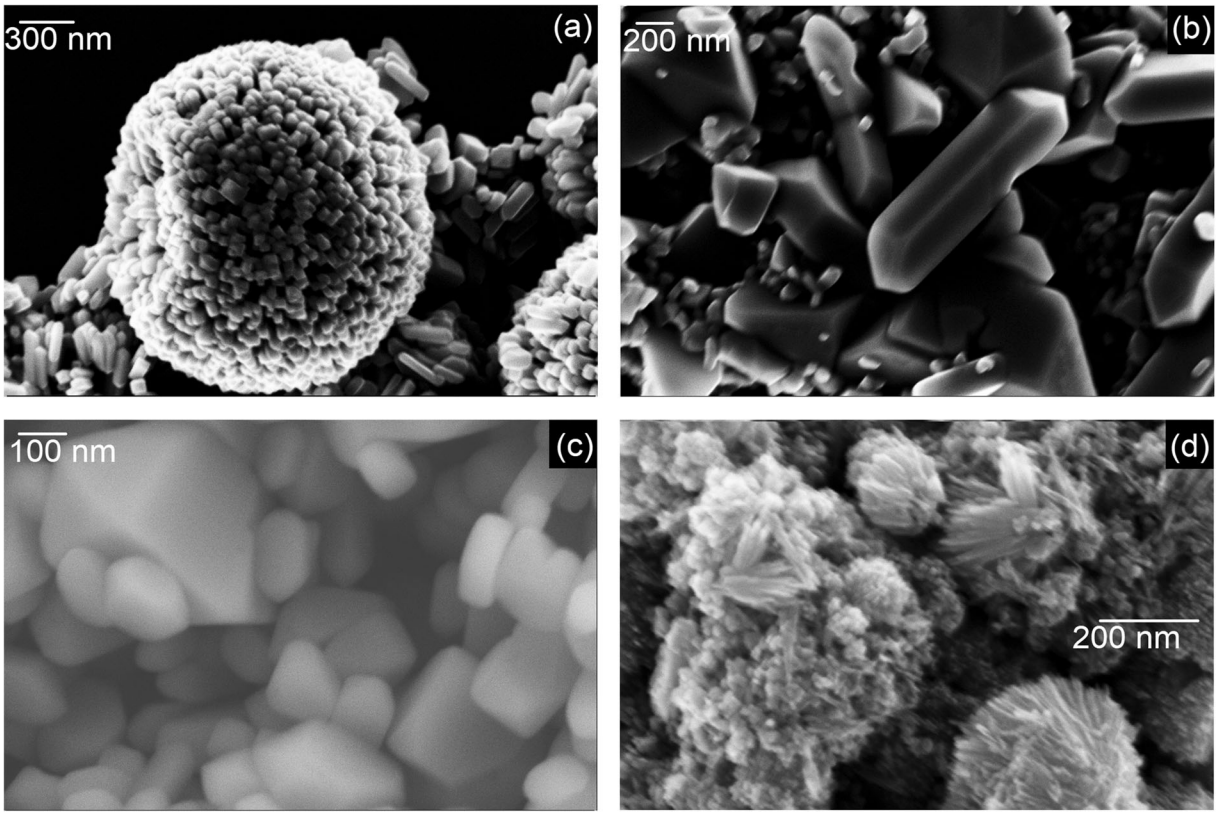

Fig. 1 SEM images of the TiO_2 nanoproducts from reaction (**a**) **4**, (**b**) **5**, (**c**) **6**, and (**d**) **8**. The product of **7** is shown later in Fig. 10

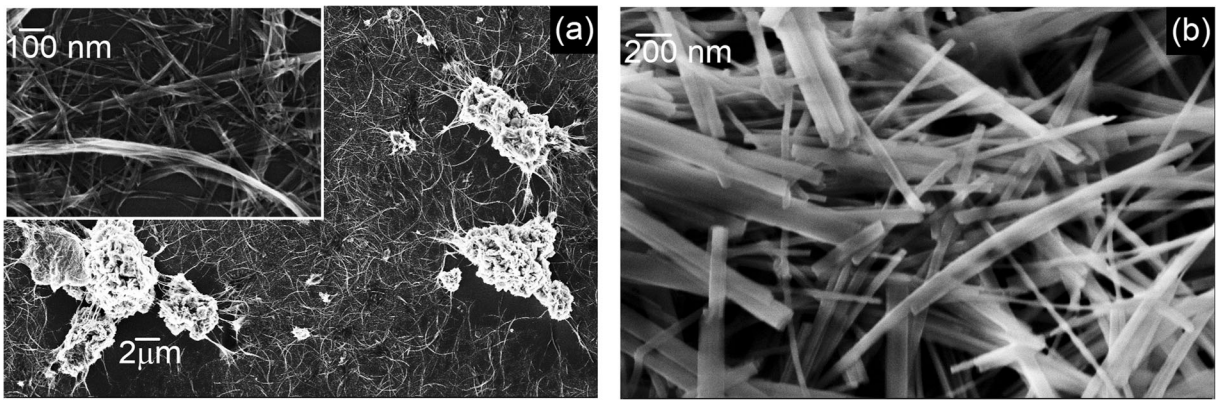

Fig. 2 SEM images of alkaline-synthesized nanowires (**a**) **9** and (**b**) **10** with the insets of the same sample at higher magnification. **11** is shown later in Fig. 12g

Vanadium oxide is known to form high aspect ratio structures easily under hydrothermal conditions (Zhang et al. 2010; Xiao et al. 2013), so ammonium vanadate was used as a precursor in acidic hydrothermal reactions, with just added acid, acid and reducing agent, or in combination with Ti or other metals. Vanadium oxide nanowires readily formed in two of the reactions, with diameters and lengths ranging from 25 to 100 nm and 2–30 μm, respectively, in **1** and **3** (Fig. 4). Reaction **2**, which used the V(III) precursor $V(OH)_2NH_2$ (Wu et al. 2011) however only formed nanocrystals. The nanowires were also shown to be either hydrous V_2O_5, V_2O_5, or VO_2 through X-ray powder diffraction (Fig. 5). Reaction **3** produced well-formed VO_2 nanowires using ethanol as a reducing agent (Wang et al. 2015). Therefore, it was hypothesized that ethanol may play a role in shape formation of other reducible metal oxides. This hypothesis was validated for tungsten when nanorod structures were produced in **17** with diameters varying from 50 to 500 nm and lengths varying from 150 to 2 μm (Fig. 4)

Vanadium was used in conjunction with titanium and other metals in **12**–**15** and **18** based on the hypothesis that vanadium would act as a nanowire structure directing agent while being substituted by other metal atoms. The expected result was nanowires that consisted of titanium-vanadium oxide for **12**–**15** and tungsten-vanadium oxide in **18**. Nanowires were produced in **12**, **14**, and **15**. In **12** and **14**, two main visible fractions resulted from the reaction; one fraction consisted of

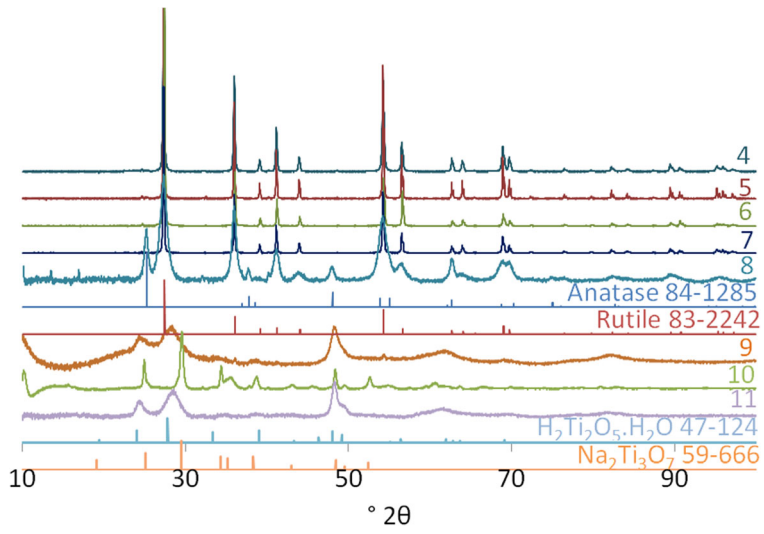

Fig. 3 XRD patterns for all titanium oxide reactions (**4**–**11**) and their comparison to Anatase, Rutile, hydrous titanium oxide, and sodium titanium oxide phases. JCPDS numbers of reference patterns are indicated on the graph

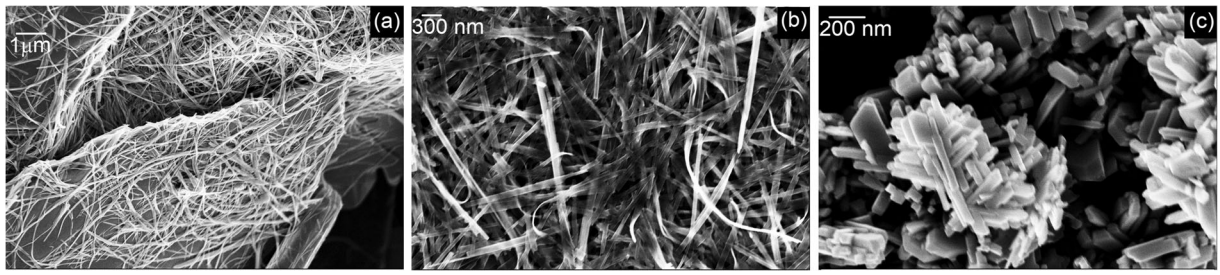

Fig. 4 SEM images of vanadium oxides (**a**) **1**, (**b**) **3**, and tungsten oxide (**c**) **17**

bright yellow solid chunks, and the other fraction was a finer conglomeration of brownish-green particles. These products (**12** and **14**) were incompletely separated into **A** and **B** fractions by washing away the finer particles in alcohol (the **B** fraction) and then sonicating the yellow solids until the conglomerations broke up into nanowires which were allowed to settle (the **A** fractions). The darker colored phase (**12B**, **14B**) was mostly of the Anatase type by XRD, while the yellowish nanowires (**12A**, **14A**) had powder patterns matching vanadium pentoxide and oxide hydrates. It was clear that elemental substitution did occur in the solid phases of **12** and **14** as can be seen in Fig. 6 and Table 3 where vanadium and titanium are both present throughout. Vanadium appears more concentrated on the mass of wires in the center of the **14** SEM/EDS map, but titanium is present also, showing that titanium is substituting into the vanadium oxide wires (Fig. 6). The EDS scan of **12** indicated similar results of titanium substituting for vanadium in some of the nanowire structures. EDS analysis of the solid products of all reactions that contained multiple metals appeared to show some substitution (Table 3). The mixed metal oxide nanowires formed from these reactions had diameters ranging from 50 to 100 nm and lengths from 2 to 28 μm (Figs. 7 and 8). The EDS analysis data showed the expected peaks for the respective elements in mixed metal nanostructures. Raman spectra (supporting information) are consistent with this phase identification. A lower concentration of NH_4VO_3 added to a titanium reaction (**13**) was not enough to sufficiently form long nanowires or rods (Fig. 8a). The addition of vanadium to a tungsten reaction also did not help nanowire formation, as **18** only formed nanoplates of irregular shapes (Fig. 8b), but single crystals of two compounds, sodium vanadate dihydrate and a POM cluster $Na_3(NH_4)_2V_3W_3O_{19}(H_2O)_{12}$, grew from the solution. The crystal structures of both compounds (supporting information) were reported previously ($NaVO_3.xH_2O$ Björnberg and Hedman 1977; Evans 1988; Kato and Takayama 1984; Lukacs and Strusievici 1962; $Na_3(NH_4)_2V_3W_3O_{19}(H_2O)_{12}$ Xu et al. 1998), and our redetermination of the POM structure was virtually identical. Our structure of $NaVO_3.2H_2O$ is very similar to the reported structures except that the previous reports show ~ 1.9 water molecules per Na, and our structure is stoichiometric. It is interesting that the POM salt

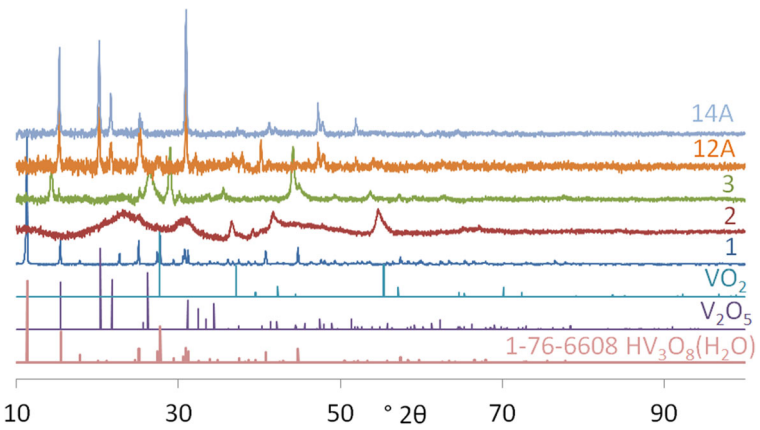

Fig. 5 XRD patterns for products **1**, **2**, **3**, **12A**, and **14A**, with matching JCPDS reference patterns indicated

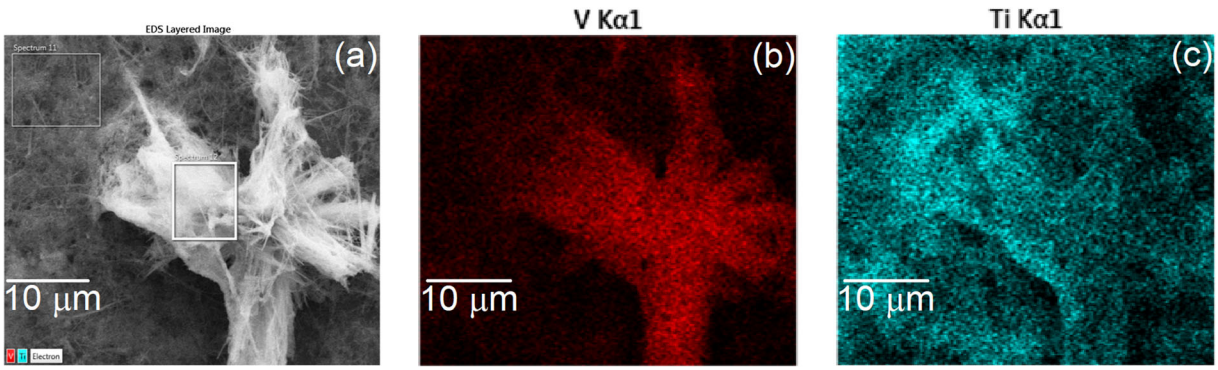

Fig. 6 Images of (**a**) SEM electron image, (**b**) EDS vanadium mapping, and (**c**) EDS titanium mapping for **14**. The clump of nanowires (**14A**) is high in vanadium, but titanium is present throughout the material

crystallizes in this stoichiometry when in principle other V-W ratios and numbers of Na and NH_4 cations should be possible. NMR and potentiometric studies have shown that solutions of tungstates and vanadates form a wide variety of polyoxometalates with different sizes and W-V ratios, although the $W_3V_3O_{19}^{5-}$ anion is favored in 50:50 mixtures (Andresson et al. 1996; Maksimovskaya et al. 1984; Rozantsev et al. 2002; Rozantsev and Sazonova 2005; Yerra et al. 2014). Even though substitution between V and W occur readily in molecular compounds, the limited amount of substitution in nanowires is likely due to the different crystal structures of the solid oxide phases.

Hydrothermal synthesis of nanowires, nanotubes, and other high aspect ratio particles of MoO_3 has been reported by many researchers (e.g., Xia et al. 2006; Muňoz-Espı et al. 2008; Dewangan et al. 2011; Hu and Wang 2008). We did one reaction (**16**), which made molybdenum oxide materials (Fig. 9). This formed very large, almost microrods with diameters and lengths extending from 0.5 to 1.5 μm and 30–100 μm (Fig. 12d). The XRD pattern of this material did not match any reference patterns exactly, but the prominent peaks did correspond to known MoO_3 phases (Fig. 9), and multiple phases are probably present.

Table 3 Composition data obtained via EDS for samples that contained multiple metals

#	Ratio
12A	V:Ti = 16.1
12B	V:Ti = 0.51
14A	V:Ti = 61.6
14B	V:Ti = 1.14
15	V:Ti = 0.23
18	W:V = 8.34

Nitridation of oxide materials

The selected products of oxide syntheses that mainly produced well-formed nanowires or rods were nitrided. The initial nitridations, where the temperature was increased very quickly under NH_3 flow (**19**, **20**), did not have very good shape retention. However, when the temperature was slowly raised, the shape retention was significantly better, and it seemed to be important to dry out the starting oxide first at low relatively low temperatures prior to nitridation. This can be illustrated by comparing the results from **20** and **21**. As seen in Figs. 10, **20** has a significant amount of fragmentation and fusion of the nanorods into tubes, and the shape retention of **21** is significantly better than **20** even though the particles are still somewhat fused together and slightly porous.

The powder patterns in Fig. 11 show that **20** was only partially nitrided, as it exhibits minor peaks for the rutile phase of TiO_2 where **21** and **22** only showed peaks for TiN. This is probably the result of more nitridation time for **21** and **22**. In general, the titanium oxides held their shape moderately well, with significant porosity and fusion of the individual rods or wires, and extensive fragmentation of thinner nanowires (Fig. 12e, f and Fig. 10). The thinnest TiO_2 nanowires (**11**) did not retain their shape at all but instead broke up and coalesced into particles (**23**) on nitridation (Fig. 12g, h). As noted above, the nitridations of vanadium oxides were also

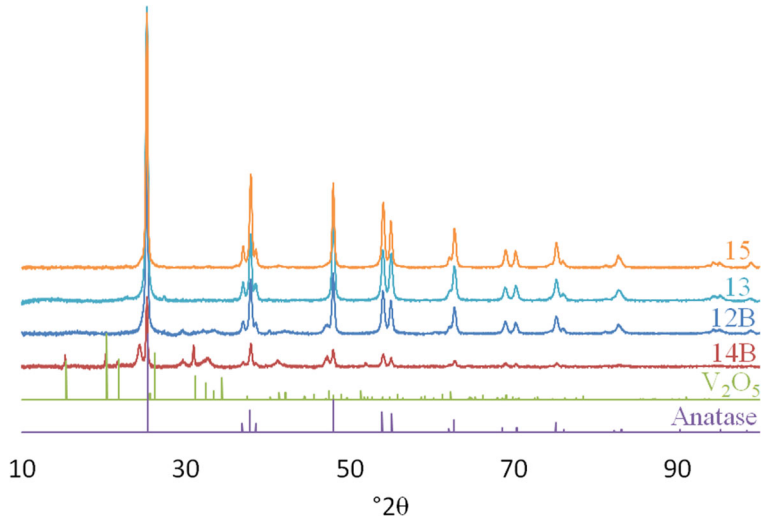

Fig. 7 Comparing **12B**, **13**, **14B**, and **15** XRD patterns to Anatase and V_2O_5 reference patterns. JCPDS reference numbers are indicated on the graph

overall more successful in shape retention when the temperature was slowly ramped up. The nitrided wires were porous, but the shape was more defined, especially in **25** (Fig. 12a–b). The vanadium nitrides **25** and **26** showed XRD peaks only for VN, while **24** still showed many peaks in the X-ray diffraction pattern for V_2O_3 (Fig. 13). Figure 12c, d also display that the molybdenum oxide nitridation product was extremely porous, almost to the point of falling apart. It still held its general shape, did not fuse together, and only shows XRD peaks for molybdenum nitrides (Fig. 13). The porous structures shown here resemble the general

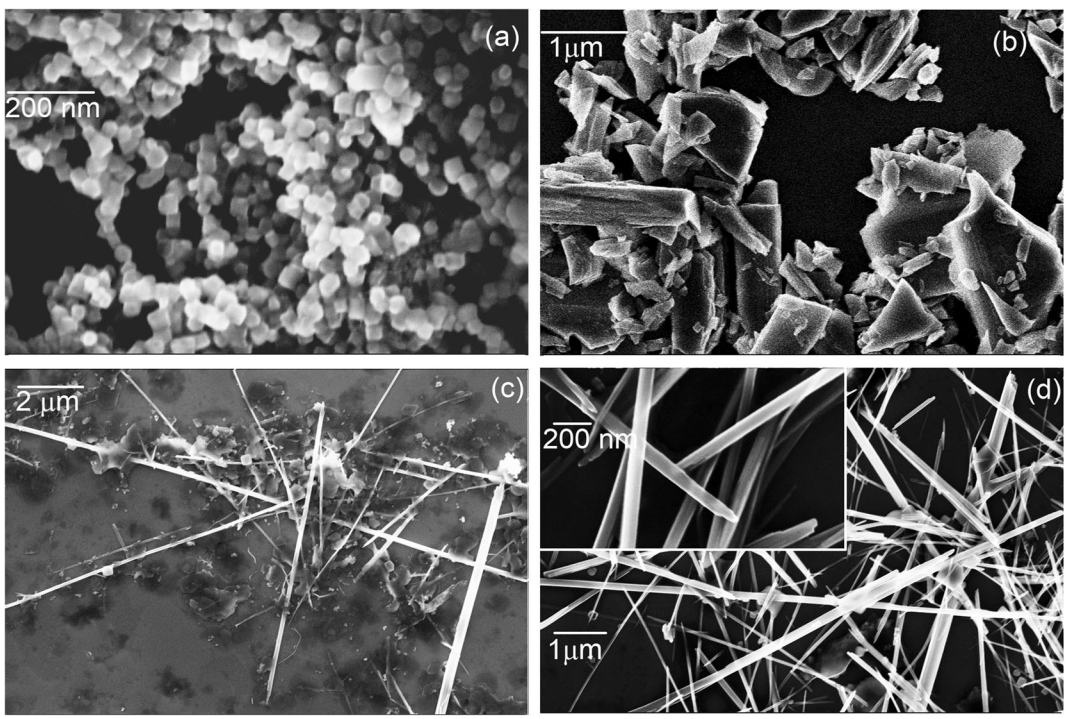

Fig. 8 SEM images of (**a**) Ti-V oxide **13**, (**b**) V-W oxide **18**, (**c**) Ti-V oxide fraction **12A**, and (**d**) Ti-V oxide fraction **14A** with inset of the same sample at higher magnification

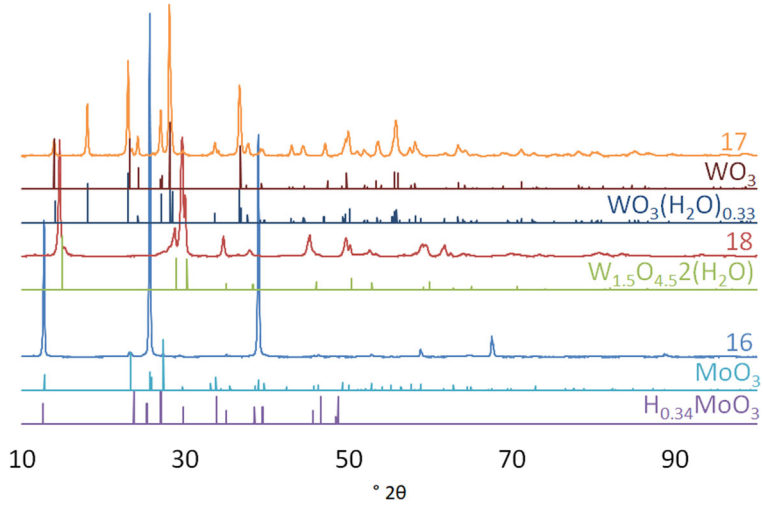

Fig. 9 XRD pattern of Mo and W oxide nanowires formed in reactions **16**, **17**, and **18** compared with JCPDS reference patterns that best corresponded to the samples

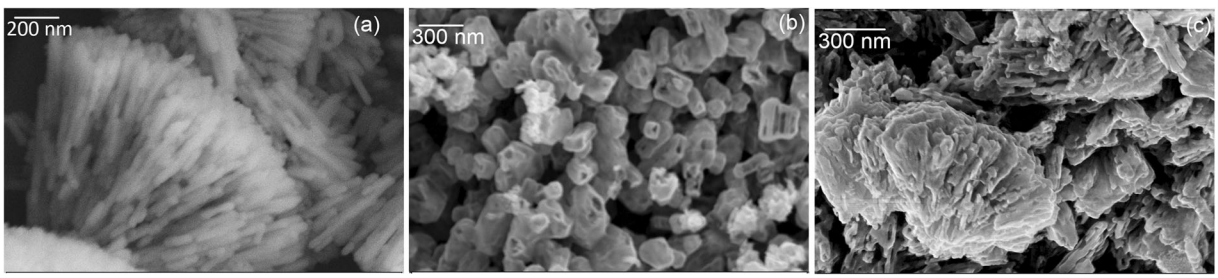

Fig. 10 SEM images of (**a**) TiO_2 nanomaterial **7**, and both TiN nanomaterials made from **7** [(**b**) **20** and (**c**) **21**], illustrating the better shape retention with slower temperature ramping rate

appearance of porous nitride structures reported by others from oxide nitridation, including Wang et al. 2015 and Lu et al. 2013.

In cases where the nitridation of any oxide was mostly complete, had reasonable shape retention, and sufficient yield, BET surface area data was taken

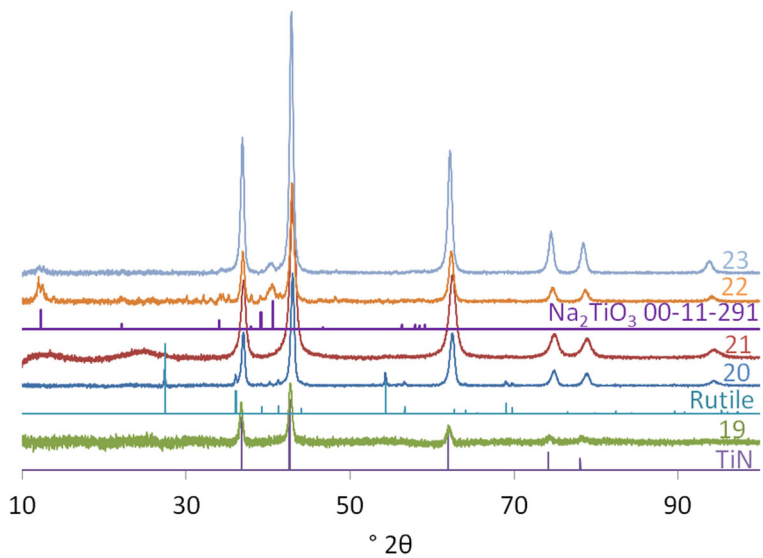

Fig. 11 Comparing XRD patterns for **19**–**23** with reference patterns for titanium nitride, rutile, and Na_2TiO_3

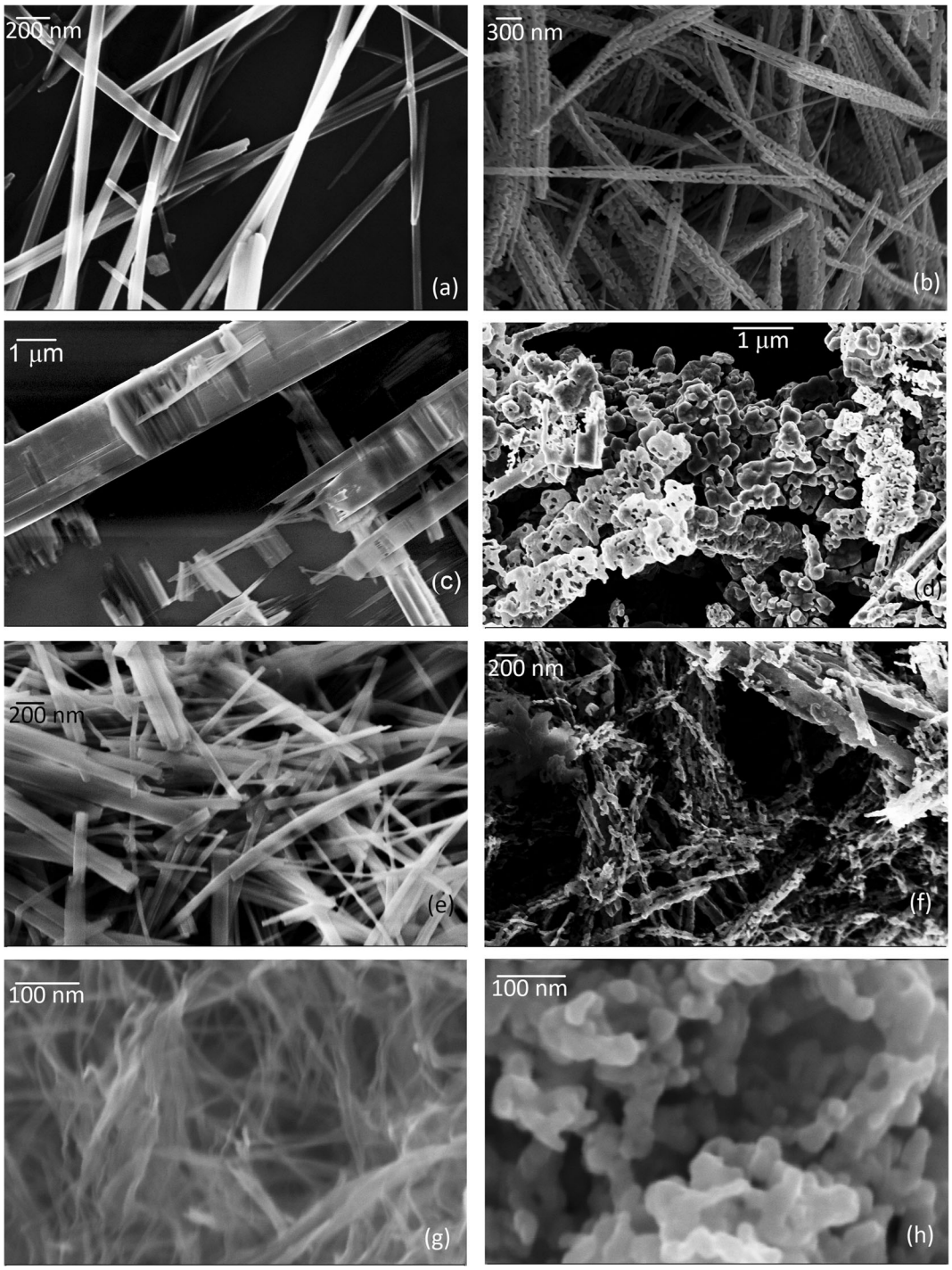

Fig. 12 SEM images of the oxide-nitride pairs: (**a**) V-Ti oxide **14A** and (**b**) nitride nanowires **25**; (**c**) MoO_3 microrods **16**, and after nitridation to Mo_2N (**d**) **27**; (**e**) $Na_2Ti_3O_7$ nanowires **10**, and after nitridation (**f**) nitride material **22**, and finally (**g**) hydrous TiO_2 nanofibers **11**, and after nitridation (**h**) to fused TiN nanoparticles **23**

(Table 4). With the exception of **26**, in general, the surface area remained approximately the same between the oxide and nitride. This was most likely due to the nanowires fusing together but becoming more porous,

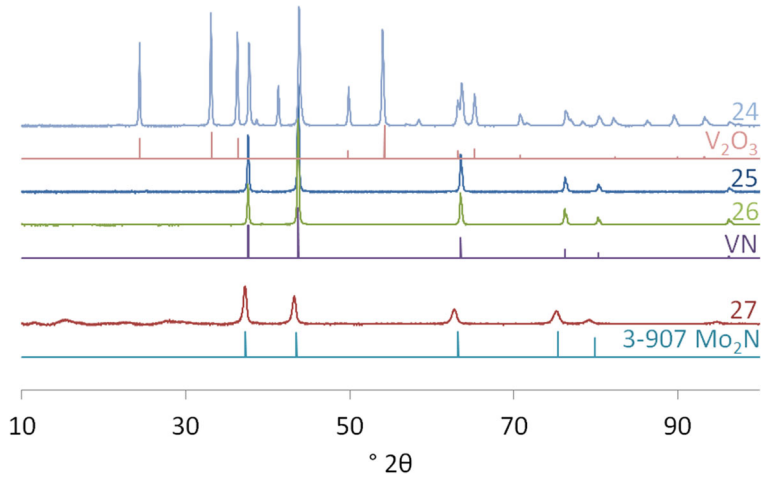

Fig. 13 XRD patterns for molybdenum and vanadium nitrides (**24**–**27**)

thus resulting in a similar overall surface area. The case of **14A** and **25** where the surface area greatly decreased from the oxide to the nitride is most likely due to the fact that the nitrided wires were not as porous as some of the other nitrides and still may have been fused or matted together.

For reactions where the nitridation was at least moderately successful in shape retention of the wires, UV-Vis and near IR data were taken in ethanol dispersions to identify the plasmon band (Fig. 14). Neither of the vanadium nitrides (**25**, **26**) nor TiN samples **21** and **22** displayed a significant plasmon band, but this could have been because they did not stay suspended in ethanol well and were highly agglomerated. No significant absorption maxima were observed for the nanowires at longer wavelengths. Nanomaterials **19** and **20** did show the characteristic plasmon band for TiN around a wavelength of 800 to 900 nm. We did not see any shift of the plasmon bands to near-infrared wavelengths due to geometry as all the spectra are consistent with the previously reported optical spectra of low aspect ratio nanoparticles (Patsalas et al. 2015; Barragan et al. 2017; Ishii et al. 2016; Guler et al. 2015; Divya et al. 2014).

Two-point bulk electrical measurements were done by pressing the nitride powders between 2 metal rods in a quartz tube, which were used as electrodes. Bulk densities of packed powders were far below the theoretical density of the nitride materials (~ 6 g/cm^3), as lots of empty space exists between the particles. The nitride powders made from acidic hydrothermally produced oxides all show metallic conductivity, as expected (Table 5). However, both of the nitride materials (**22** and **23**) prepared from the alkaline hydrothermal synthesized oxides (**10** and **11**) showed semiconductivity, very high capacitance (high effective dielectric constants), and high dissipation factors. The most likely reason for this behavior is incomplete conversion to nitride, leaving thin layers of dielectric material coating the nitride crystallites. The X-ray diffraction patterns of these two materials show small extra peaks between 12 and 40.5° that most closely matches Na_2TiO_3 (Fig. 11). Also, the Raman spectra (supporting information) show extra peaks in **22** and **23** that are not present in the other TiN samples. The precursor material **11** also shows high dielectric constants with even higher dissipation factors,

Table 4 BET surface area data for samples 3 and 26, 10 and 22, 14A and 25, and 16 and 27

#	Phase	BET surface area $\left(\frac{m^2}{g}\right)$
3	VO_2, V_2O_5	45
26	VN	1
10	$Na_2Ti_3O_7$	21
22	TiN	21
14A	V_2O_5, $H_{0.39}V_2O_5$	44
25	VN	20
16	$H_{0.34}MoO_3$, MoO_3	4
27	Mo_2N	5

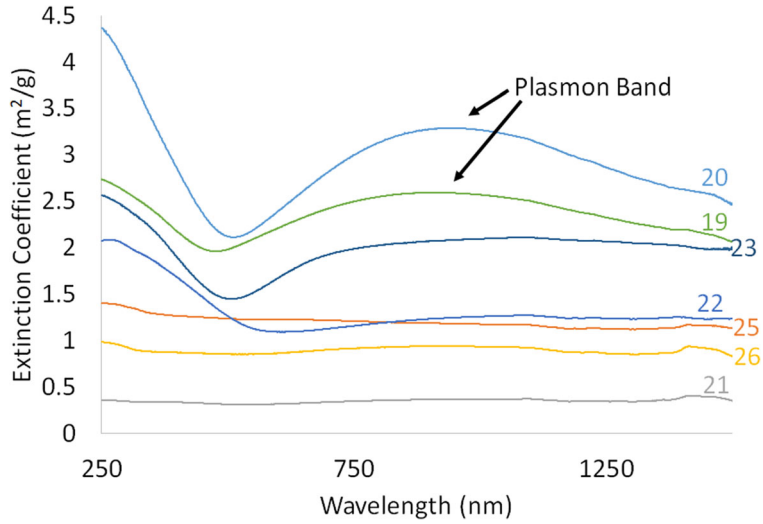

Fig. 14 UV-Vis spectra of nitrides **19**–**23**, **25**, and **26** dispersed in ethanol

probably a result of the OH groups in the material. Nitride and oxide nanowire films on electrodes have been used in electrochemical capacitors (Liu et al. 2016; Dhananjaya et al. 2018; Wang et al. 2016; Liu et al. 2020), and this result demonstrates the possibility of these materials being used for dry capacitor technology as well.

Conclusions

Nanowires and nanorods of Ti, V, and Mo oxides are readily grown under acidic hydrothermal conditions. While some elemental substitution of these metals does occur within the oxide structures when mixtures of metals are present in solution, the amount of substitution appears to be minimal. Nanoparticles of the oxides of Ti, V, Mo, and W are readily converted to their respective nitrides by heating under flowing NH_3 up to 900 °C. Maximum shape retention for high aspect ratio nanostructures (nanowires) is best achieved by dehydration below 200 °C followed by slowly increasing the nitridation temperature. With V and Mo, a general feature of such nitrided nanowires is porosity, and with Ti fusion and fragmentation of the nanowires was observed, and most prominent with the thinnest nanowires. The most intact, although porous, nitride nanowires were produced from vanadium pentoxide nanowires

Table 5 Resistivity, dielectric constant, and dissipation factor measurements on nitride products

#	DC resistivity (Ω-m)	ε', D (1 KHz)	ε', D (120 Hz)	Sample density (g/cm^3)
11	No stable reading	5900, 20	162,000, 5.5	0.30
19	1E-3 (metallic)			1.2
20	0.7E-3 (metallic)			0.96
21	1E-3 (metallic)			1.1
22	2150	55,000, 2.9	230,000, 3.6	0.70
23	425	47,000, 3.9	259,000, 4.5	0.70
24	<1E-3 (metallic)			0.82
25	4E-3 (metallic)			0.78
26	<1E-3 (metallic)			0.97
27	2E-3 (metallic)			1.4

that had a small amount of titanium present, and these nanowires showed metallic conductivity. These results should enable methods of inexpensive bulk production of conductive nanowires for a wide variety of technologies, even if the high porosity precludes applications that require fully consolidated nanowires.

Acknowledgments We thank the Office of Naval Research for financial support.

Compliance with ethical standards

Conflict of interest The authors declare that they have no conflict of interest.

References

Andresson I, Hastings JJ, Howarth OW, Petterson L (1996) Aqueous tungstovanadate equilibria. J Chem Soc Dalton Trans 1996:2705–2711

Barragan AA, Ilawe NV, Zhong L, Wong BM, Mangolini L (2017) A non-thermal plasma route to plasmonic TiN nanoparticles. J Phys Chem C 121:2316–2322

Björnberg A, Hedman B (1977) The crystal structure of $NaVO_3$.1.89H_2O. Acta Chemica Scandanavica A 31:579–584

Cassaignon S, Koelsch M, Jolivet J (2007) Selective synthesis of brookite, anatase and rutile nanoparticles: thermolysis of $TiCl_4$ in aqueous nitric acid. J Mater Sci 42:6689–6695

Chen X, Mao SS (2007) Titanium dioxide nanomaterials: synthesis, properties, modifications, and applications. Chem Rev 107:2891–2959

Dewangan K, Sinha NN, Sharma PK, Pandey AC, Munichandraiah N, Gajbhiye NS (2011) Synthesis and characterization of single-crystalline a-MoO_3 nanofibers for enhanced Li-ion intercalation applications. CrystEngComm 13: 927–933

Dhananjaya M, Prakash NG, Narayana AL, Hussain OM (2018) Microstructural and supercapacitive properties of one-dimensional vanadium pentoxide nanowires synthesized by hydrothermal method. Applied Physics A 124:185

Ding J, Dengn C, Yuann W, Zhu H, Li J (2013) The synthesis of titanium nitride whiskers on the surface of graphite by molten salt media. Ceram Int 39:2995–3000

Divya S, Nampoori VPN, Radhakrishnan P, Mujeeb A (2014) Origin of optical non-linear response in TiN owing to excitation dynamics of surface plasmon resonance electronic oscillations. Laser Phys Lett 11:085401

Drygas M, Czosnek C, Paine RT, Janik JJ (2006) Two-stage aerosol synthesis of titanium nitride TiN and titanium oxynitride TiO_xN_y nanopowders of spherical particle morphology. Chem Mater 18:3122–3129

Evans HT (1988) The crystallography of munirite, $NaVO_3$.(2-x)H_20. Mineral Mag 52:716–717

Fei L, Yongdi L, Yadong Y, Hao Z, Wei S, Yunqing K, Guangfu Y, Zhongbing H, Xiaoming L, Xiaofeng L (2011) Preparation of titanium nitride nanoparticles from a novel refluxing derived precursor. Journal of Wuhan University of Technology-Mater Sci Ed 26:429–433

Gou H, Zhang G, Chou K (2017) Phase evolution and reaction mechanism during reduction–nitridation process of titanium dioxide with ammonia. J Mater Sci 52:1255–1264

Guler U, Suslov S, Kildishev AV, Boltasseva A, Shalaev VM (2015) Colloidal plasmonic titanium nitride nanoparticles: properties and applications. Nanophotonics 4:269–276

Hirao I, Hasegawa A (2010) Titania nanotubes and a method of manufacturing the same. JP4525149B2, Aug. 18th 2010

Howell IR, Giroire B, Garcia A, Li S, Aymonier C, Watkins JJ (2018) Fabrication of plasmonic TiN nanostructures by nitridation of nanoimprinted TiO_2 nanoparticles. J Mater Chem C 6:1399–1406

Hu S, Wang X (2008) Single-walled MoO_3 nanotubes. J Am Chem Soc 130:8126–8127

Ishii S, Shinde SL, Jevasuwan W, Fukata N, Nagao T (2016) Hot electron excitation from titanium nitride using visible light. ACS Photonics 3:1552–1557

Joshi UA, Chung SH, Lee JS (2005) Low-temperature, solvent-free solid-state synthesis of single-crystalline titanium nitride nanorods with different aspect ratios. J Solid State Chem 178: 55–760

Kato VK, Takayama E (1984) Das Entwässerungsverhalten des Natriummetavanadatdihydrats und die Kristallstruktur des ß-Natriummetavanadats. Acta Cryst B40:102–105

Lang K, Klein M, Domann G, Löbmann P (2020) Transparent conductive organic–inorganic hybrid composites based on Ag nanowires. J Sol-Gel Sci Technol 96:121–129. https://doi.org/10.1007/s10971-020-05330-y

Lengauer W, Binder S, Aigner K, Ettmayer P, Guillou A, Debuigne J, Groboth G (1995) Solid state properties of group IVb carbonitrides. J Alloys Compounds 217:137–147

Lerch M (1996) Nitridation of Zirconia J Am Ceram Soc 79:2641–2644

Lin G, Xi S, Pan C, Lin W, Xie K (2018) Growth of 2 cm metallic porous TiN single crystals. Mater Horiz 5:953–960

Liu Y, Xiao R, Qiu Y, Fang Y, Zhang P (2016) Flexible advanced asymmetric supercapacitors based on titanium nitride-based nanowire electrodes. Electrochim Acta 213:393–399

Liu X, Liu H, Sun X (2020) Aligned ZnO nanorod@Ni–Co layered double hydroxide composite nanosheet arrays with a core–shell structure as high-performance supercapacitor electrode materials. CrystEngComm 22:1593–1601

Lu X, Yu M, Zhai T, Wang G, Xie S, Liu T, Liang C, Tong Y, Li Y (2013) High energy density asymmetric quasi-solid-state supercapacitor based on porous vanadium nitride nanowire anode. Nano Lett 13:2628–2633

Lukacs VI, Strusievici C (1962) Uber die polymorphie von natriummetavanadat. Z Anorg Allg Chem 315:323–326

Maksimovskaya RI, Il'yasova AK, Begalieva DU, Takezhanova DF, Akhmetova AK (1984) Identification of mixed vanadium-tungsten polooxocomplexes in aqueous solutions by ^{17}O and ^{51}V NMR. Izvestiya Akademii Nauk SSSR, Seriya Khimicheskaya, 1984: 2169–74

Mangamma G, Ajikumar PK, Nithya R, Sairam TN, Mittal VK, Kamruddin M, Dash S, Tyagi AK (2007) Synthesis and gas phase nitridation of nanocrystalline TiO_2. J Phys D Appl Phys 40:597–4602

Mosavati N, Chitturi VR, Salley SO, Ng KYS (2016) Nanostructured titanium nitride as a novel cathode for high performance lithium/dissolved polysulfide batteries. J Power Sources 321:87–93

Mosavati N, Salley SO, Ng KYS (2017) Characterization and electrochemical activities of nanostructured transition metal nitrides as cathode materials for lithium sulfur batteries. J Power Sources 340:210–216

Muñoz-Espı R, Burger C, Krishnan CV, Chu B (2008) Polymer-controlled crystallization of molybdenum oxides from peroxomolybdates: structural diversity and application to catalytic epoxidation. Chem Mater 20:7301–7311. https://doi.org/10.1021/cm802193t

Patsalas P, Kalfagiannis N, Kassavetis S (2015) Optical properties and plasmonic performance of titanium nitride. Materials 8: 3128–3154

Perales-Martínez IA, Rodríguez-González V (2017) Towards the hydrothermal growth of hierarchical cauliflower-like TiO2 anatase structures. J Sol-Gel Sci Technol 81:741–749

Poudel B, Wang WZ, Dames C, Huang JY, Kunwar S, Wang DZ, Banerjee D, Chen G, Ren ZF (2005) Formation of crystallized titania nanotubes and their transformation into nanowires. Nanotechnology 16:1935–1940

Qiu Y, Yan K, Yang S, Jin L, Deng H, Li W (2010) Synthesis of size-tunable anatase TiO_2 nanospindles and their assembly into anatase@titanium oxynitride/titanium nitride graphene nanocomposites for rechargeable lithium ion batteries with high cycling performance. ACS Nano 4:6515–6526

Rozantsev GM, Sazonova OI (2005) State of the ions and synthesis of isopoly compounds from vanadotungstate solutions at a vanadium-to-tungsten ratio of 3:3. Russ J Inorg Chem 50: 1974–1980

Rozantsev GM, Sazonova OI, Kholin YV (2002) Mathematical modeling of pH-potentiometric measurements in tungsten-vanadium solutions. Russian J Phys Chem 76:384–390

Sharma R, Naedele D, Schweda E (2001) In situ studies of nitridation of zirconia (ZrO_2). Chem Mater 13:4014–4018

Song J, Li GR, Xi K, Lei B, Gao XP, Kumar RV (2014) Enhancement of diffusion kinetics in porous MoN nanorods-based counter electrode in a dye sensitized solar cell. J Mater Chem A 2:10041–10047

Tan BJ, Xiao Y, Galasso FS, Suib SL (1994) Thermodynamic analysis and synthesis of zirconium nitride by thermal nitridation of sol-gel zirconium oxide. Chem Mater 6:918–926

Vallant T, Brunner H, Mayer U, Hoffmann H (1998) Control of structural order in self-assembled zirconium Alkylphosphonate films. Langmuir 14:5826–5833

Wang X, Li Z, Shi J, Yu Y (2014) One-dimensional titanium dioxide nanomaterials: nanowires, nanorods, and nanobelts. Chem Rev 114:9346–9384

Wang R, Lang J, Zhang P, Lin Z, Yan X (2015) Fast and large lithium storage in 3D porous VN nanowires–graphene composite as a superior anode toward high-performance hybrid supercapacitors. Adv FunctMater 25:2270–2278

Wang B, Chen Z, Lu G, Wang T, Ge Y (2016) Exploring electrolyte preference of vanadium nitride supercapacitor electrodes. Mater Res Bull 76:37–40

Wei M, Qi Z, Ichihara M, Hirabayashi M, Honma I, Zhou H (2006) Synthesis of single-crystal vanadium dioxide nanosheets by the hydrothermal process. J Cryst Growth 296:1–5

Wu C, Zhang X, Dai J, Yang J, Wu Z, Wei S, Xie Y (2011) Direct hydrothermal synthesis of monoclinic VO_2(M) single-domain nanorods on large scale displaying magnetocaloric effect. J Mater Chem 21:4509–4517

Xia T, Li Q, Liu X, Meng J, Cao X (2006) Morphology-controllable synthesis and characterization of single-crystal molybdenum trioxide. J Phys Chem B 110:2006–2012

Xiao X, Peng X, Jin H, Li T, Zhang C, Gao B, Hu B, Huo K, Zhou J (2013) Freestanding mesoporous VN/CNT hybrid electrodes for flexible all-solid-state supercapacitors. Adv Mater 25:5091–5097

Xihong L, Lu X, Yu M, Zhai T, Wang G, Xie S, Liu T, Liang C, Tong Y, Li Y et al (2013) High energy density asymmetric quasi-solid-state supercapacitor based on porous vanadium nitride nanowire anode. Nano Lett 13:2628–2633

Xu Y, Xu J, Yang G, Wang T, Xing Y, Lin Y, Jia H (1998) $(NH_4)_2Na_3(V_3W_3O_{19}).12H_2O$. Acta Cryst C 54:563–565

Yerra S, Amanchi SR, Das SK (2014) Synthesis and structural characterization of Lindqvist type mixed-metal cluster anion $[V_2W_4O_{19}]^{4-}$ in discrete and coordination polymer compounds. J Mol Struct 1062:53–60

Yu CC, Ramanathan S, Oyama ST (1998) New catalysts for hydroprocessing: bimetallic oxynitrides M_I–M_{II}–O–N (M_I, M_{II} = Mo, W, V, Nb, Cr, Mn, and Co). J Catal 173:1–9 No. CA971887

Zhang R, Engholm M (2018) Recent progress on the fabrication and properties of silver nanowire-based transparent electrodes. Nanomaterials 8:628

Zhang Y, Liu X, Xie G, Yu L, Yi S, Hu M, Huang C (2010) Hydrothermal synthesis, characterization, formation mechanism and electrochemical property of $V_3O_7{\cdot}H_2O$ single-crystal nanobelts. Mater Sci Eng B 175:164–171

Zhang L, Bu J, Wei H, Chen M, Liu H, Ni J, Lv D (2017) Synthesis and electrochemical properties of porous tubular TiN powders prepared via ammonia reduction nitridation of nonhydrolytic TiO_2 powders. J Ceram Soc Jpn 125:628–633

Zhou W, Liu X, Cui J, Liu D, Li J, Jiang H, Wang J, Liu H (2011) Control synthesis of rutile TiO_2 microspheres, nanoflowers, nanotrees and nanobelts via acid-hydrothermal method and their optical properties. CrystEngComm 13:4557–4563

Zhou L, Yang L, Shao L, Chen B, Meng F, Qian Y, Xu L (2017) General fabrication of boride, carbide, and nitride nanocrystals via a metal-hydrolysis-assisted process. Inorg Chem 56:2440–2447